

NJC

Accepted Manuscript



This is an *Accepted Manuscript*, which has been through the Royal Society of Chemistry peer review process and has been accepted for publication.

Accepted Manuscripts are published online shortly after acceptance, before technical editing, formatting and proof reading. Using this free service, authors can make their results available to the community, in citable form, before we publish the edited article. We will replace this *Accepted Manuscript* with the edited and formatted *Advance Article* as soon as it is available.

You can find more information about *Accepted Manuscripts* in the [Information for Authors](#).

Please note that technical editing may introduce minor changes to the text and/or graphics, which may alter content. The journal's standard [Terms & Conditions](#) and the [Ethical guidelines](#) still apply. In no event shall the Royal Society of Chemistry be held responsible for any errors or omissions in this *Accepted Manuscript* or any consequences arising from the use of any information it contains.

Transition metal phosphonates with supramolecular structures: syntheses, structures, surface photovoltage and luminescent properties

Yan-Yu Zhu, Mei-Ling Wang, Ming-Xue Ma, Zhen-Gang Sun,* Cheng-Qi Jiao, Chao Ma and Huan-Yu Li

Four new transition metal phosphonates with 2D and 3D supramolecular structures, namely, $[\text{Cu}_2(1,10\text{-phen})_2(\text{HL})_2(\text{L})]\cdot\text{H}_2\text{L}$ (**1**), $[\text{Zn}(1,10\text{-phen})(\text{HL})_2]$ (**2**), $[\text{M}(1,10\text{-phen})(\text{HL})_2(\text{H}_2\text{L})]$ ($\text{M} = \text{Mn}$ (**3**), Cd (**4**)) ($\text{H}_2\text{L} = \text{phenylphosphonic acid}$, $1,10\text{-phen} = 1,10\text{-phenanthroline}$), have been synthesized under hydrothermal conditions. In compound **1**, two $\{\text{CuN}_2\text{O}_3\}$ square pyramids and three $\{\text{CPO}_3\}$ tetrahedra are interconnected through phosphonate oxygen atoms to form a cluster unit *via* edge- and corner-sharing. Neighboring units are further assembled into a 3D supramolecular structure through $\pi\text{-}\pi$ stacking and hydrogen bonding interactions. For compound **2**, two $\{\text{ZnO}_3\text{N}_2\}$ square pyramids and four $\{\text{CPO}_3\}$ tetrahedra are interconnected by phosphonate oxygen atoms to a cluster unit *via* corner-sharing. Then the adjacent clusters are further assembled into a 3D supramolecular structure through $\pi\text{-}\pi$ stacking interactions. Compounds **3** and **4** are isomorphous and adopt a 2D supramolecular structure through $\pi\text{-}\pi$ stacking interactions. The interconnection of $\{\text{MO}_4\text{N}_2\}$ and $\{\text{CPO}_3\}$ polyhedra leads to a cluster unit through corner-sharing, and such units are further assembled into a 2D supramolecular structure by $\pi\text{-}\pi$ stacking and hydrogen bonding interactions. The surface photovoltage properties of compounds **1**, **3** and luminescent properties of compounds **2**, **4** have been studied. The surface photovoltage spectra (SPS) and field-induced surface photovoltage spectra (FISPS) of compounds **1** and **3** indicate that they all possess certain photo-electric conversion properties and show *p*-type semiconductor characteristics. Luminescent properties of compounds **2** and **4** indicate that they may be candidates for potential luminescent materials.

Introduction

Supramolecular chemistry, beyond molecular chemistry, based on self-assembly of molecular building blocks has received considerable interest mainly due to its fascinating structural properties and potential applications in ion exchanging, catalysis, medicine and materials chemistry.¹

School of Chemistry and Chemical Engineering, Liaoning Normal University, Dalian 116029, P. R. China.

E-mail: szg188@163.com

In supramolecular materials, the molecular building blocks are self-organized *via* noncovalent interactions, such as intermolecular hydrogen-bonding, aromatic π - π stacking interactions, charge groups and non-bonding electronic repulsion, and these weaker intermolecular forces play a significant role in increasing the dimensionality of polymerization.² As an important part of supramolecular chemistry, metal phosphonate compounds have also attracted much attention on account of their structural diversities and exhibit a wide range of unique properties.³ Therefore, the rational design and synthesis of novel metal phosphonates with intriguing supramolecular structures and practical properties have become a particularly important subject. An important and useful strategy of building new types of metal phosphonate hybrids with supramolecular structures is to introduce a second organic ligand such as oxalate, carboxylic acid, 2,2'-bipyridine, 4,4'-bipyridine, or 1,10-phenanthroline into the structures of metal phosphonates.⁴ In recent years, a number of transition metal phosphonates have been isolated, and results from ours and other groups indicate that the introduction of a second organic ligand has been proved to be an effective synthetic method of transition metal phosphonates with new structure types and interesting properties.⁵ In view of photoelectric property, phosphonic acids containing an aromatic ring may be useful ligands due to their rigidity and large π -conjugated system. During the past few years, a series of supramolecular compounds of copper with bi- and tridentate amines and phenylphosphonic acids have been reported by K. Latham et al.⁶ The phenylphosphonic acids in most of these compounds have been used in the context of intermolecular design in addition to the well known use of phosphonates in co-ordination networks. In this paper, we selected phenylphosphonic acid (H₂L) as the phosphonate ligand and 1,10-phenanthroline as the second metal linker. Our research efforts resulted in four new transition metal phosphonates with 2D and 3D supramolecular structures, namely, [Cu₂(1,10-phen)₂(HL)₂(L)]·H₂L (**1**), [Zn(1,10-phen)(HL)₂] (**2**), [M(1,10-phen)(HL)₂(H₂L)] (M = Mn (**3**), Cd (**4**)), and the surface photovoltage properties of compounds **1**, **3** and the luminescent properties of compounds **2**, **4** have also been studied. At present, research on the properties of transition metal phosphonates is mainly focused on magnetism, luminescence, proton conductivity and ion exchange *etc*, and there are seldom reports on the surface photovoltage property.⁷ Surface photovoltage spectroscopy (SPS) is a well-established contactless and nondestructive technique for the characterization of semiconductors or materials with semiconducting properties. SPS is not only relates to the charge transition process under light inducement but also reflects directly the separation and transition of photogenerated charges.⁸ The energy gaps of some transition metal

compounds are sometimes in the region of the gaps of semiconductors. This phenomenon means that they can show certain semiconductor characteristic and therefore be considered as some type of inorganic–organic hybrid semiconductors. The study on the electronic behavior of valence shell and photovoltaic performance of transition metal compounds will provide special references for further research on the functions of these compounds. Recently, only a few investigations on the surface photovoltage property of metal phosphonates have been reported by our group.⁹ Herein we report the syntheses, crystal structures, surface photovoltage and luminescent properties of four title compounds.

Experimental

Materials and measurements

The phenylphosphonic acid was purchased from Shanghai Kaisai Chemical Co., Ltd. All chemicals were used as obtained without further purification. C, H and N content was determined by using a PE–2400 elemental analyzer. Cu, Zn, Mn, Cd and P content was determined by using an inductively coupled plasma (ICP) atomic absorption spectrometer. IR spectra were recorded on a Bruker AXS TENSOR–27 FT–IR spectrometer with KBr pellets in the range 4000–400 cm^{-1} . The X–ray powder diffraction data was collected on a Bruker AXS D8 Advance diffractometer using Cu–K α radiation ($\lambda = 1.5418 \text{ \AA}$) in the 2θ range of 5–60° with a step size of 0.02° and a scanning rate of 3°/min. Thermogravimetric (TG) analyses were performed on a Perkin–Elmer Pyris Diamond TG–DTA thermal analyses system in static air with a heating rate of 10 K min^{-1} from 50 to 900°C. The luminescence analyses were performed on a HITACHI F–7000 spectrofluorimeter. Surface photovoltage spectroscopy (SPS) and field–induced surface photovoltage spectroscopy (FISPS) measurements were conducted with the sample in a sandwich cell (ITO/sample/ITO) using the light source–monochromator–lock–in detection technique in the range of 300–600 nm.

Syntheses

General procedure. By using phenylphosphonic acid (H_2L) as the phosphonate ligand and 1,10–phenanthroline as a second metal linker, four new transition metal phosphonates with mixed ligands have been synthesized under hydrothermal conditions. Product composition depends on a number of critical conditions, including the initial reactants, molar ratio, pH value, reaction time

and temperature in the process of hydrothermal synthesis. With the aim to explore the optimum method for obtaining pure phase materials, two systematic experimental investigations have been designed. For compound **1**, the first experiment was designed to investigate the influence of the anions of copper salts on the reaction products. Thus, four different copper salts ($\text{CuCl}_2 \cdot 2\text{H}_2\text{O}$, $\text{Cu}(\text{Ac})_2 \cdot \text{H}_2\text{O}$, $\text{Cu}(\text{NO}_3)_2 \cdot 3\text{H}_2\text{O}$ and $\text{CuSO}_4 \cdot 5\text{H}_2\text{O}$) were reacted keeping a constant $\text{Cu}^{2+} : 1,10\text{-phen} : \text{H}_2\text{L} = 1 : 1 : 5$ ratio at their original pH ($T = 120\text{ }^\circ\text{C}$, 72 h). Our experiments demonstrated that the final reaction products synthesized from different copper salts exhibit different phases. $\text{CuCl}_2 \cdot 2\text{H}_2\text{O}$ (original pH = 3), $\text{Cu}(\text{Ac})_2 \cdot \text{H}_2\text{O}$ (original pH = 4) and $\text{Cu}(\text{NO}_3)_2 \cdot 3\text{H}_2\text{O}$ (original pH = 2) acting as reactants synthesize amorphous powders. However, mixture phases (colorless crystals and powder) for compound **1** are obtained using $\text{CuSO}_4 \cdot 5\text{H}_2\text{O}$ (original pH = 2.5). So we realize that $\text{CuSO}_4 \cdot 5\text{H}_2\text{O}$ may be the more adaptable copper salt to use as the reactant to synthesize compound **1**. In addition, the reaction temperature also has a strong effect on the formation of the compounds. To gain a better understanding of the influence of the reaction temperature, a second experiment was designed. The system using $\text{CuSO}_4 \cdot 5\text{H}_2\text{O}$ as the copper salt at different temperature was studied. Larger crystals of compound **1** were obtained at the reaction temperature of $100\text{ }^\circ\text{C}$. However, the formation of amorphous powders or mixture phases for compound **1** comes into being at other temperatures. Compound **1** can also be obtained at $120\text{ }^\circ\text{C}$ and $140\text{ }^\circ\text{C}$, but the quality is not good enough for single-crystal structure determination. The results of the two experimental investigations indicate that $\text{CuSO}_4 \cdot 5\text{H}_2\text{O}$ is the optimal copper salt to synthesize the pure phase of single crystals for compound **1** at a constant $\text{Cu}^{2+} : 1,10\text{-phen} : \text{H}_2\text{L} = 1 : 1 : 5$ ratio at the reaction temperature of $100\text{ }^\circ\text{C}$. Analogous experimental investigations were also designed to obtain the optimum method for synthesizing compounds **2–4**. It is unnecessary to adjust the pH values of the reaction mixtures for the syntheses of these compounds. The powder XRD patterns and the simulated XRD patterns of the four compounds are shown in the ESI (Fig. S1–S3, ESI). The diffraction peaks on the patterns correspond well in position, confirming that the four compounds are in pure phase. The differences in reflection intensity are probably due to the preferred orientation in the powder samples.

[Cu₂(1,10-phen)₂(HL)₂(L)]·H₂L (1). A mixture of $\text{CuSO}_4 \cdot 5\text{H}_2\text{O}$ (0.12 g, 0.50 mmol), H_2L (0.40 g, 2.50 mmol) and 1,10-phen (0.10 g, 0.50 mmol) was dissolved in 10 mL distilled water. The resulting solution was stirred for about 1h at room temperature, sealed in a 20 mL Teflon-lined stainless steel autoclave, and heated at 100°C for 3 days under autogenous pressure. After the

mixture was cooled slowly to room temperature, the blue block crystals of **1** were obtained. Yield 49.2 % (based on Cu). Anal. Calc. for $C_{48}H_{40}N_4O_{12}P_4Cu_2$: C, 51.67; H, 3.61; N, 5.02; P, 11.10; Cu, 11.39. Found: C, 51.63; H, 3.63; N, 5.06; P, 11.06; Cu, 11.43 %. IR (KBr, cm^{-1}): 3073(m), 1588(m), 1517(m), 1442(m), 1308(w), 1137(s), 1101(s), 943(s), 850(s), 750(m), 699(s), 556(s), 442(m).

[Zn(1,10-phen)(HL)₂] (**2**). A mixture of $Zn(Ac)_2 \cdot 2H_2O$ (0.11 g, 0.50 mmol), H_2L (0.40 g, 2.50 mmol) and 1,10-phen (0.10 g, 0.50 mmol) was dissolved in 10 mL distilled water. The resulting solution was stirred for about 1h at room temperature, sealed in a 20 mL Teflon-lined stainless steel autoclave, and heated at 120°C for 3 days under autogenous pressure. After the mixture was cooled slowly to room temperature, the colorless block crystals of **2** were obtained. Yield 52.1 % (based on Zn). Anal. Calc. for $C_{24}H_{20}N_2O_6P_2Zn$: C, 51.50; H, 3.60; N, 5.00; P, 11.07; Zn, 11.68. Found: C, 51.46; H, 3.63; N, 4.95; P, 11.12; Zn, 11.63 %. IR (KBr, cm^{-1}): 3070(w), 1617(w), 1528(w), 1517(w), 1432(m), 1309(m), 1180(m), 1130(s), 1043(s), 943(m), 908(m), 843(w), 750(m), 727(m), 699(m), 563(s), 527(m), 506(w), 455(w).

[Mn(1,10-phen)(HL)₂(H₂L)] (**3**). A mixture of $Mn(Ac)_2 \cdot 4H_2O$ (0.12 g, 0.50 mmol), H_2L (0.40 g, 2.50 mmol) and 1,10-phen (0.10 g, 0.50 mmol) was dissolved in 10 mL distilled water. The resulting solution was stirred for about 1h at room temperature, sealed in a 20 mL Teflon-lined stainless steel autoclave, and heated at 180°C for 3 days under autogenous pressure. After the mixture was cooled slowly to room temperature, the yellow block crystals of **3** were obtained. Yield 40.3 % (based on Mn). Anal. Calc. for $C_{30}H_{27}N_2O_9P_3Mn$: C, 50.94; H, 3.85; N, 3.96; P, 13.14; Mn, 7.77. Found: C, 50.91; H, 3.88; N, 3.92; P, 13.19; Mn, 7.73 %. IR (KBr, cm^{-1}): IR (KBr, cm^{-1}): 3056(w), 1627(w), 1591(w), 1519(w), 1426(m), 1232(m), 1189(s), 1138(s), 1068(m), 1016(s), 916(s), 844(m), 752(m), 726(w), 693(m), 548(s), 521(s), 449(w), 420(w).

[Cd(1,10-phen)(HL)₂(H₂L)] (**4**). The procedure was the same as that for **3** except that $Mn(Ac)_2 \cdot 4H_2O$ was replaced by $CdCl_2 \cdot 2.5H_2O$ (0.11 g, 0.50 mmol). The colorless block crystals of **4** were obtained. Yield 23.8 % (based on Cd). Anal. Calc. for $C_{30}H_{27}N_2O_9P_3Cd$: C, 47.11; H, 3.56; N, 3.66; P, 12.15; Cd, 14.70. Found: C, 47.15; H, 3.53; N, 3.69; P, 12.10; Cd, 14.75 %. IR (KBr, cm^{-1}): 3049(w), 1621(w), 1591(w), 1426(m), 1347(w), 1147(s), 1031(m), 925(m), 916(m), 858(m), 752(w), 723(w), 696(m), 557(m), 515(m), 456(w), 420(w).

X-Ray crystallography

Data collections for compounds **1–4** were performed on the Bruker AXS Smart APEX II CCD X-diffractometer equipped with graphite monochromated MoK α radiation ($\lambda = 0.71073 \text{ \AA}$). An empirical absorption correction was applied using the SADABS program. All structures were solved by direct methods and refined by full matrix least-squares fitting on F^2 by SHELXL-2014/7.¹⁰ Anisotropic thermal parameters were applied to all non-hydrogen atoms. Hydrogen atoms of organic ligands were generated geometrically with fixed isotropic thermal parameters and included in the structure factor calculations. Details of crystallographic data of compounds **1–4** are summarized in Table 1. Hydrogen bonds for compounds **1**, **3** and **4** are given in Table 2. Selected bond lengths and angles of compounds **1–4** are listed in Table S1–S3 (ESI). CCDC 1043125–1043128 contain the supplementary crystallographic data for this paper. These data can be obtained free of charge www.ccdc.cam.ac.uk/conts/retrieving.html (or from the Cambridge Crystallographic Data Center, 12, Union Road, Cambridge CB21EZ, UK; fax: (+44) 1223-336-033; e-mail: deposit@ccdc.cam.ac.uk).

Results and discussion

Description of the crystal structures

Description of structure 1. Compound **1** crystallizes in the triclinic space group $P\bar{1}$ (see Table 1). As shown in Fig. 1, each asymmetric unit contains two crystallographically unique Cu(II) ions, two HL⁻ anions, one L²⁻ anion, two 1,10-phen molecules and one free H₂L molecule. Both Cu(II) ions hold {CuN₂O₃} square pyramid coordination geometries. Cu1 ion is five-coordinated by three phosphonate oxygen atoms (O1, O4, O7) from two HL⁻ anions and one L²⁻ anion, two nitrogen atoms (N1, N2) from one 1,10-phen molecule. Cu2 ion is also five-coordinated by three phosphonate oxygen atoms (O1, O6, O7) from two HL⁻ anions and one L²⁻ anion, two nitrogen atoms (N3, N4) from one 1,10-phen molecule. The bond lengths of Cu–O and Cu–N are in the range of 1.907(2)–2.296(2) Å and 1.999(3)–2.027(3) Å, respectively (Table S1, ESI), which are comparable to those reported for other copper(II) phosphonates.¹¹ The coordination modes of the three phosphonic acid ligands can be described as bidentate bridging modes (Fig. 2a, 2b and 2c). The phosphonate oxygen atoms (O3 and O9) of HL⁻ anions are protonated based on the requirement of charge balance.

The overall structure of compound **1** can be described as a 3D supramolecular structure. As shown in Fig. 3, each {CPO₃} tetrahedron connects two {CuN₂O₃} square pyramids through phosphonate oxygen atoms, and the {CuN₂O₃} square pyramids are interconnected by {CPO₃} tetrahedra *via* edge- and corner-sharing to form a [Cu₂(1,10-phen)₂(HL)₂(L)] cluster unit. Such neighboring units are assembled into a 2D layer through π - π stacking interactions. The π - π stacking interactions can play an important role in controlling the packing or assembly of compounds. The usual π interaction is an offset or slipped stacking of the aromatic nitrogen heterocycles or benzene rings, and the effective distance is about 3.3–3.8 Å.¹² In compound **1**, the 1, 10-phen rings between the neighboring units are parallel to each other, and the face-to-face distances (3.68 Å and 3.65 Å) between adjacent 1, 10-phen rings are in the normal range for such interactions; hence the units are connected through π - π stacking interactions to form a 1D chain. Meanwhile, the chains are assembled into a 2D supramolecular layer through π - π stacking interactions between the adjacent benzene rings with the face-to-face distance of 3.73 Å. The free phenylphosphonate molecules are located between the units. The phosphorus atom (P4) and the phosphonate oxygen atoms (O10, O11 and O12) in the free phenylphosphonate molecule appeared to be disordered over two sites (occupancies 0.6 and 0.4) respectively. There are four types of hydrogen bonds between the free phenylphosphonate oxygen atoms and the uncoordinated phosphonate oxygen atoms. The O \cdots O distances are 2.490(10), 2.371(10), 2.435(14) and 2.652(15) Å for O(3)-H(3) \cdots O(12)#1, O(3)-H(3) \cdots O(12')#1, O(10)-H(10) \cdots O(8)#2 and O(11)-H(11) \cdots O(9)#2, respectively. The interactions contribute in forming a 3D supramolecular structure (see Fig. 4 and Table 2)

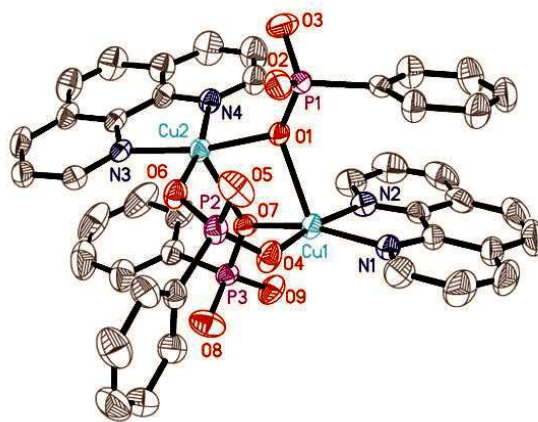


Fig. 1 Structure unit of compound **1** showing the atom labeling. Thermal ellipsoids are shown at the 50% probability level. All H atoms and the free H₂L molecule are omitted for clarity

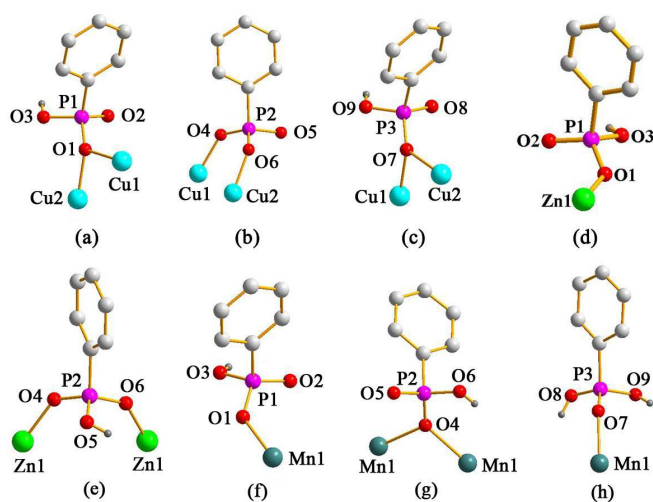


Fig. 2 The coordination modes of phosphonate ligands in compound **1** (a), (b) and (c); compound **2** (d) and (e); compound **3** (f), (g) and (h).

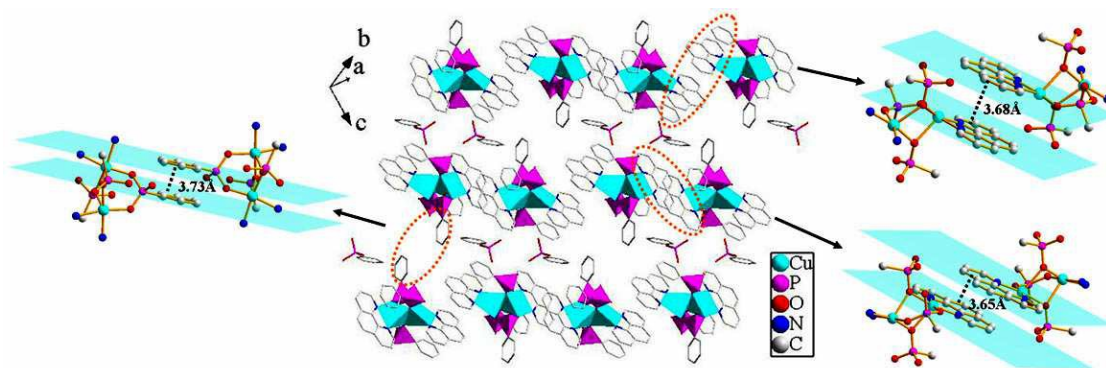


Fig. 3 A view of the 2D supramolecular structure *via* the π - π stacking interactions for compound **1**. The π - π stacking interactions between the adjacent 1,10-phen and benzene rings with the face-to-face distances of 3.68 Å, 3.65 Å and 3.73 Å.

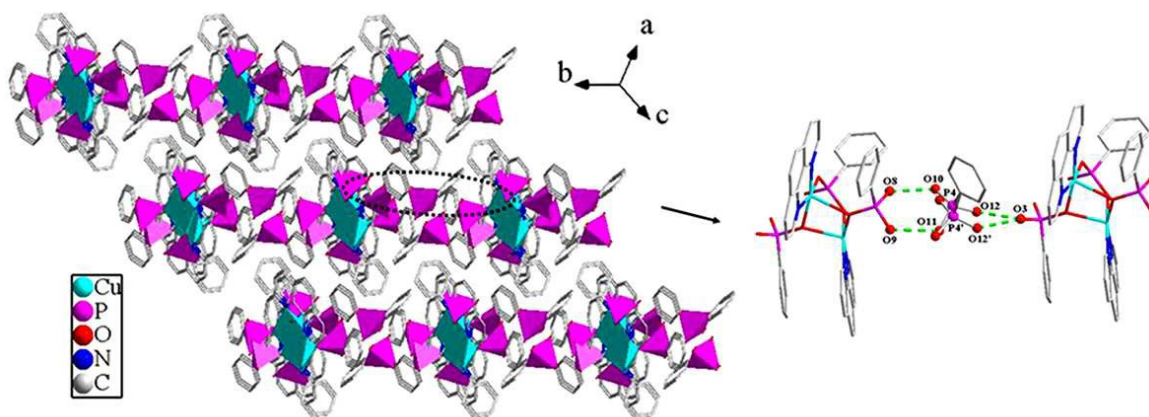


Fig. 4 The three-dimensional supramolecular structure of compound **1**. Hydrogen bonds are drawn as dotted green lines.

Table 1 Crystal data and structure refinement for compounds **1–4**.

Compounds	1	2	3	4
Chemical formula	C ₄₈ H ₄₀ N ₄ O ₁₂ P ₄ Cu ₂	C ₂₄ H ₂₀ N ₂ O ₆ P ₂ Zn	C ₃₀ H ₂₇ N ₂ O ₉ P ₃ Mn	C ₃₀ H ₂₇ N ₂ O ₉ P ₃ Cd
Formula weight	1115.80	559.75	707.39	764.84
Crystal system	Triclinic	Triclinic	Monoclinic	Monoclinic
Space group	<i>P</i> -1	<i>P</i> -1	<i>P</i> 2(1)/ <i>c</i>	<i>P</i> 2(1)/ <i>c</i>
<i>a</i> /Å	12.1430(13)	11.1636(6)	13.0305(8)	13.1419(6)
<i>b</i> /Å	14.0076(14)	11.3733(6)	14.3151(9)	14.4775(7)
<i>c</i> /Å	14.3167(14)	11.8809(6)	17.8602(10)	17.4996(8)
α°	107.833(2)	105.5630(10)	90	90
β°	93.586(2)	114.9730(10)	111.826(4)	110.4410(10)
γ°	92.363(2)	103.1950(10)	90	90
<i>V</i> /Å ³	2309.0(4)	1212.38(11)	3092.7(3)	3119.9(3)
<i>Z</i>	2	2	4	4
<i>D</i> _{calc} /g cm ⁻³	1.605	1.533	1.519	1.628
<i>F</i> (000)	1140	572	1452	1544
μ /mm ⁻¹	1.130	1.188	0.639	0.911
θ range /deg	1.499 to 26.499	2.020 to 26.499	1.683 to 26.498	1.654 to 26.498
Reflections collected	12935	7011	17508	17697
Unique reflections	9382 [R _{int} = 0.0245]	4955 [R _{int} = 0.0131]	6410 [R _{int} = 0.0235]	6474 [R _{int} = 0.0252]
Completeness	98.9 %	99.1 %	100.0 %	99.9 %
Goodness of fit on <i>F</i> ²	1.016	1.042	1.015	1.021
<i>R</i> ₁ , <i>wR</i> ₂ [<i>I</i> > 2σ(<i>I</i>)]	0.0475, 0.1204	0.0266, 0.0666	0.0321, 0.0813	0.0318, 0.0729
<i>R</i> ₁ , <i>wR</i> ₂ (all data)	0.0761, 0.1390	0.0319, 0.0698	0.0478, 0.0901	0.0444, 0.0804
$\delta\rho_{\max}$, $\delta\rho_{\min}$ /e Å ⁻³	1.248, -0.524	0.340, -0.360	0.292, -0.279	0.604, -0.568
$R_1 = \Sigma (F_0 - F_C) / \Sigma F_0 $, $wR_2 = [\Sigma w (F_0 - F_C)^2 / \Sigma w F_0^2]^{1/2}$.				

Table 2 Hydrogen bond distances (Å) and angles (°) for compounds **1**, **3** and **4**

Compound 1				
D–H...A	D(D–H)/ Å	d(H...A)/ Å	D–H...A/ °	d(D...A)/ Å
O(3)–H(3)...O(12)#1	0.82	1.68	168.3	2.490(10)
O(3)–H(3)...O(12')#1	0.82	1.72	134.2	2.371(10)
O(10)–H(10)...O(8)#2	0.82	1.66	157.7	2.435(14)
O(11)–H(11)...O(9)#2	0.82	1.85	164.5	2.652(15)
Symmetry transformations used to generate equivalent atoms: #1 –x + 1, –y, –z + 1; #2 –x + 1, –y + 1, –z + 1.				
Compound 3				
D–H...A	D(D–H)/ Å	d(H...A)/ Å	D–H...A/ °	d(D...A)/ Å
O(3)–H(3)...O(2)#2	0.82	1.80	167.2	2.608(2)
Symmetry transformations used to generate equivalent atoms: #2 –x + 1, –y + 2, –z.				
Compound 4				
D–H...A	D(D–H)/ Å	d(H...A)/ Å	D–H...A/ °	d(D...A)/ Å
O(3)–H(3A)...O(2)#2	0.82	1.79	163.4	2.589(3)
Symmetry transformations used to generate equivalent atoms: #2 –x + 1, –y + 2, –z.				

Description of structure 2. Compound **2** crystallizes in the triclinic space group $P\bar{1}$ (see Table 1). The asymmetric unit contains one Zn(II) ion, two HL^- anions and one 1,10–phen molecule (Fig. 5). Zn1 ion is five–coordinated to give a $\{\text{ZnO}_3\text{N}_2\}$ square pyramid coordination geometry. Three of the five coordination positions are filled with three phosphonate oxygen atoms (O1, O4, O6A) from three HL^- anions. The remaining sites are occupied by two nitrogen atoms (N1, N2) from one 1, 10–phen molecule. The Zn–O [1.9599(13)–2.0326(13) Å] and Zn–N [2.1241(16)–2.2143(16) Å] distances are comparable to those in other reported zinc(II) phosphonates (Table S2, ESI).¹³ One of the phosphonic acid ligands acts as a monodentate ligand and another acts as a bidentate ligand (Fig. 2d and 2e). Based on the charge balance, the phosphonate oxygen atoms (O3 and O5) in HL^- anions are protonated.

Compound **2** shows a 3D supramolecular network. As shown in Fig. 6, two $\{\text{ZnO}_3\text{N}_2\}$ polyhedra are interconnected by four $\{\text{CPO}_3\}$ tetrahedra through phosphonate oxygen atoms to form a $[\text{Zn}_2(1,10\text{-phen})_2(\text{HL})_4]$ cluster unit *via* corner–sharing. These neighboring units are further connected through π – π stacking interactions to result in a 2D supramolecular layer in *ac*–plane. The

average face-to-face distances of the aromatic units are about 3.55 Å (between the adjacent 1, 10-phen rings) and 3.59 Å (between the adjacent benzene rings), which are within the range of π - π stacking interactions (3.3–3.8 Å), hence there exist π - π stacking interactions. Meanwhile, the neighboring layers are further assembled into a 3D supramolecular structure through π - π stacking interactions between the adjacent benzene rings with the face-to-face distance of 3.55 Å (Fig. 7).

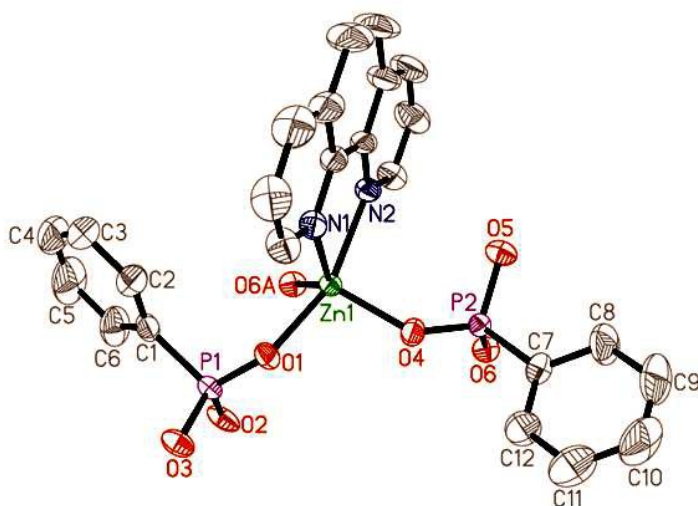


Fig. 5 Structure unit of compound **2** showing the atom labeling. Thermal ellipsoids are shown at the 50% probability level. All H atoms are omitted for clarity. Symmetry code for the generated atoms: (A) $-x, -y, -z$.

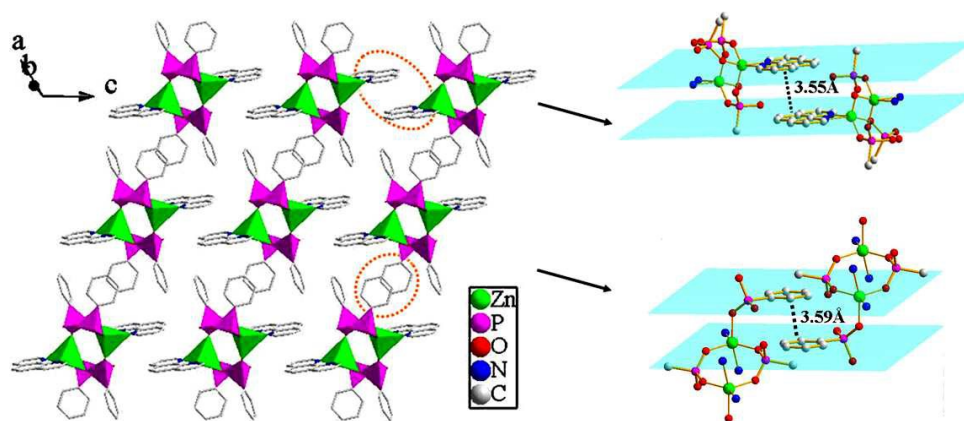


Fig. 6 A view of the 2D supramolecular structure *via* the π - π stacking interactions for compound **2**. The π - π stacking interactions between the adjacent 1, 10-phen and benzene rings with the face-to-face distances of 3.55 Å and 3.59 Å.

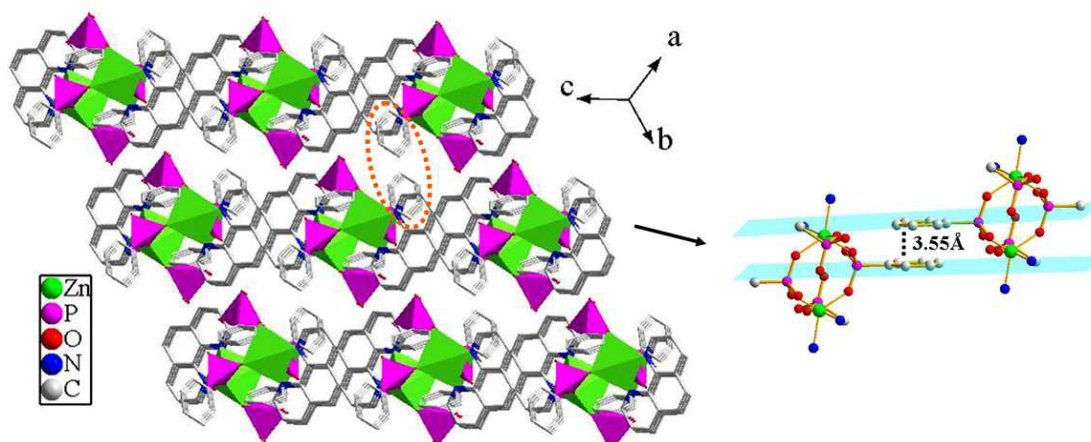


Fig. 7 The three-dimensional supramolecular structure of compound **2** via the π - π stacking interactions. The π - π stacking interactions between the adjacent benzene rings with the face-to-face distance of 3.55 Å.

Description of structure 3. Single-crystal X-ray diffraction analysis reveals that compounds **3** and **4** are isostructural and crystallize in the monoclinic $P2(1)/c$ space group (see Table 1). Hence only the structure of compound **3** will be discussed in detail as a representation. There is one Mn(II) ion, two HL^- anions, one H_2L molecule and one 1,10-phen molecule in the asymmetric unit of compound **3** (Fig. 8). Mn1 ion is six-coordinated by four oxygen atoms (O1, O4, O4A, O7) from three separate HL^- anions and one H_2L molecule, and two nitrogen atoms (N1, N2) from one 1,10-phen molecule. The bond lengths of Mn-O and Mn-N are in the range of 2.1163(13)–2.2188(13) Å and 2.2837(16)–2.3551(17) Å, respectively (Table S3, ESI), which are comparable to those reported for other manganese(II) phosphonates.¹⁴ In compound **3**, three phosphonic acid ligands display three different kinds of coordination modes, and the carbon atoms (C8, C9 and C10) in one of the HL^- anions appeared to be disordered over two sites (occupancies 0.47 and 0.53) respectively. The phosphonate oxygen atoms (O3 and O6) of HL^- anions and the phosphonate oxygen atoms (O8 and O9) of H_2L molecule are protonated based on the requirement of charge balance (Fig. 2f, 2g and 2h).

The overall structure of compound **3** can be described as a 2D supramolecular structure. As shown in Fig. 9, two $\{\text{MnO}_4\text{N}_2\}$ polyhedra and six $\{\text{CPO}_3\}$ tetrahedra are linked through phosphonate oxygen atoms via edge- and corner-sharing to form a $[\text{Mn}_2(1,10\text{-phen})_2(\text{HL})_4(\text{H}_2\text{L})_2]$ cluster unit. The neighboring units are assembled into a 1D chain along the b -axis through π - π

stacking interactions with the average face-to-face distance between the aromatic units (phen) of 3.72 Å. These neighboring chains are further connected through hydrogen bonding interactions to give rise to a 2D supramolecular structure. There are hydrogen bonds between the uncoordinated phosphonate oxygen atoms (O2 and O3) with distance of 2.608(2) Å (O3–H3...O2#2) and corresponding angle of 167.2° (symmetry transformations used to generate equivalent atoms: #2 – x + 1, – y + 2, – z) (Table 2).

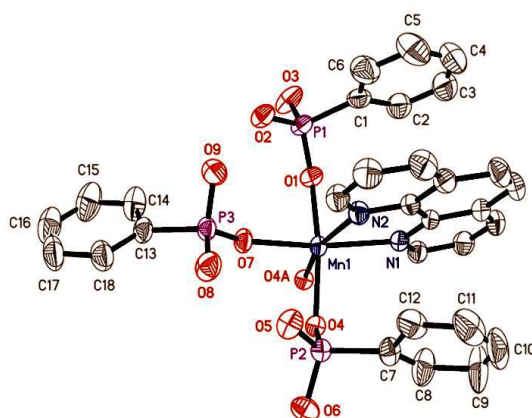


Fig. 8 Structure unit of compound **3** showing the atom labeling. Thermal ellipsoids are shown at the 50% probability level. All H atoms and the disordered carbon atoms (C8', C9' and C10') are omitted for clarity. Symmetry code for the generated atoms: (A) – x, – y + 2, – z.

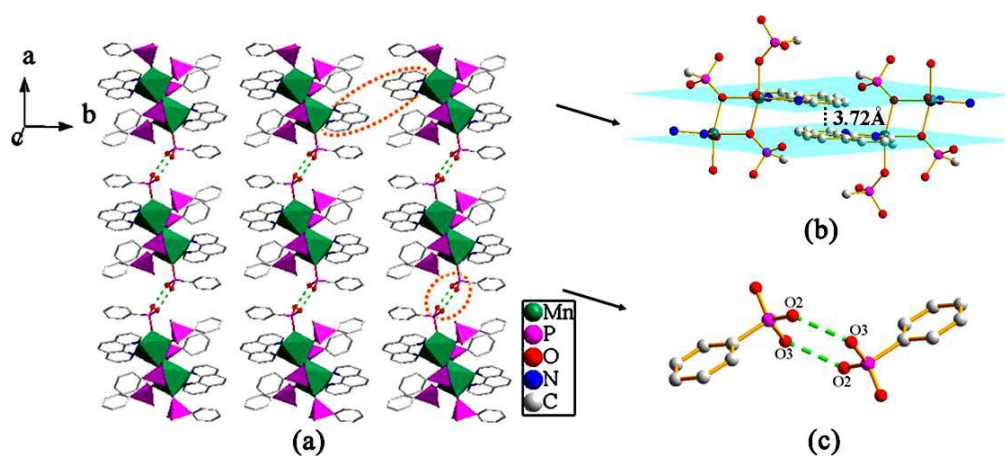


Fig. 9 (a) A view of the 2D supramolecular structure for compound **3**. (b) The π – π stacking interactions between the adjacent 1, 10–phen rings with the face-to-face distance of 3.72 Å. (c) The connectivity of hydrogen bonds. Hydrogen bonds are drawn as dotted green lines.

IR spectra

The IR spectra for compounds **1–4** are recorded in the region 4000–400 cm^{-1} (Fig. S4–S6, ESI). Compounds **3** and **4** are isostructural, they have many similar features corresponding to their common groups. Thus only the IR spectra of compounds **1–3** will be discussed. The C–H stretching vibrations are observed as sharp, weak bands close to 3000 cm^{-1} for compounds **1–3**. Absorption bands at 1588, 1517 and 1442 cm^{-1} for **1**, 1582, 1517 and 1432 cm^{-1} for **2**, 1591, 1519 and 1426 cm^{-1} for **3** can be attributed to the stretching bands of the 1,10–phenanthroline ligands.¹⁵ The bands at 750, 699 cm^{-1} for **1**, 750, 727, 699 cm^{-1} for **2** and 752, 726, 693 cm^{-1} for **3** are due to the out-of-plane CH vibrations of C_6H_5 , and are characteristic of phenylphosphonates in general.¹⁶ Strong bands between 1200 and 900 cm^{-1} for three compounds are due to stretching vibrations of the tetrahedral $\{\text{CPO}_3\}$ groups, as expected.¹⁷ Additional medium and weak bands at low energies for compounds **1–3** are found, which are likely assigned to bending vibrations of the tetrahedral $\{\text{CPO}_3\}$ groups.

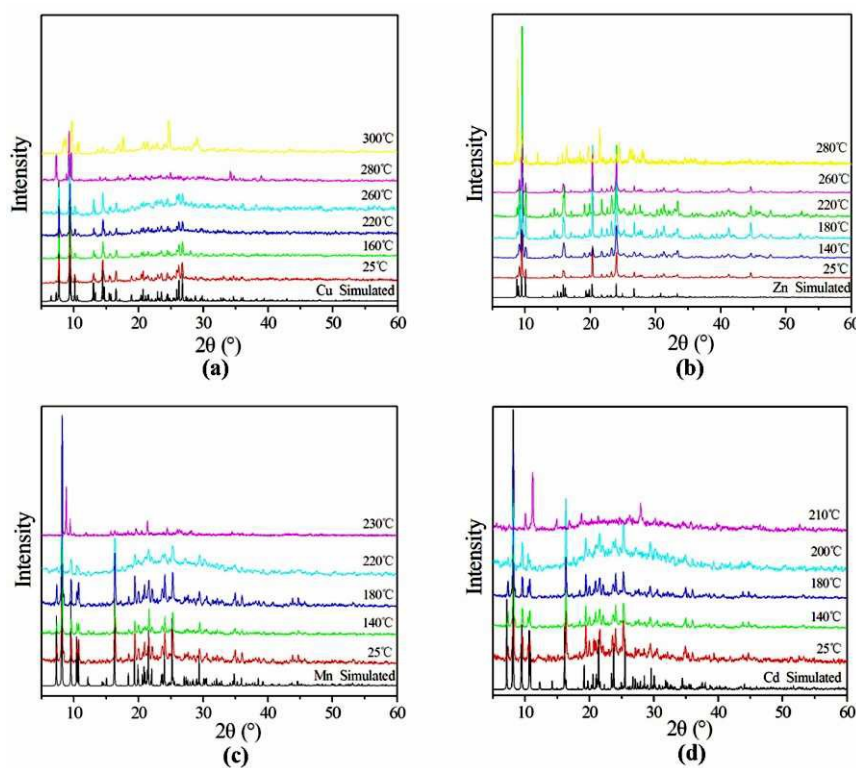


Fig. 10 PXRD patterns for (a) **1** on heating from 25 to 300°C, (b) **2** on heating from 25 to 280°C, (c) **3** on heating from 25 to 230°C and (d) **4** on heating from 25 to 210°C.

Thermal analysis

In order to examine the thermal stabilities of compounds **1–4**, thermogravimetric analyses were performed in the temperature range of 50–900 °C in static air atmosphere (Fig. S7–S10, ESI). Compound **1** was thermally stable up to a high temperature of 270 °C. Above this temperature, the TG curve shows three main continuous weight losses. At approximately 300 °C, it completes its first step of weight loss, corresponding to the partial decomposition of the free phenylphosphonate molecule. A second weight loss occurs between 352 and 530 °C, which can be attributed to the further decomposition of the free phenylphosphonate molecule, the partial decomposition of the organic moieties and the collapse of the structures. The third stage occurring between 530 and 790 °C corresponds to the further decomposition of the compound. The total weight loss of 59.5% is almost consistent with the calculated value (60.3%) if the final products are assumed to be $\text{Cu}(\text{PO}_3)_2$. We try to confirm the supposition by PXRD, but the final residues are unidentified because they are amorphous. The TG curve of compound **2** reveals two main steps of weight losses. The first step exhibits a continuous and complicated weight loss between 272 °C and 608 °C, which can be attributed to the combustion of organic groups and the collapse of the structures. The second step, from 608 to 825 °C, corresponds to the further decomposition of the compound. The final product was not characterized because they are amorphous. The total weight loss of 63.5% is basically consistent with the calculated value (60.1%) if the final products are assumed to be $\text{Zn}(\text{PO}_3)_2$. The TG curve of compound **3** exhibits a main continuous weight loss in the temperature range 192–725 °C, which can be attributed to the elimination of the organic moieties and the collapse of the structures. The final product of the thermal process is $\text{Mn}(\text{PO}_3)_2$ (JCPDS 00–029–0892) on the basis of powder X–ray diffraction (Fig. S11, ESI). The total weight loss of 63.6% is smaller than the calculated value (69.9%), because of an amorphous product (black glassy carbon) existing at the same time. Compound **4** exhibits a continuous and complicated weight loss in the temperature range 215–800 °C, which corresponds to the pyrolysis of the organic moieties and the collapse of the structures. For compound **4**, the final product of the thermal decomposition is amorphous and was not further characterized. The total weight loss of 61.4% is basically close to the calculated value (64.6%) if the final product is assumed to be $\text{Cd}(\text{PO}_3)_2$ at 800 °C.

To further understand the thermal stability of these compounds, X–ray powder diffraction studies were performed for the as–synthesized compounds and the samples heated 160–300 °C for compound **1**, 140–280 °C for compound **2**, 140–230 °C for compound **3** and 140–210 °C for

compound **4** for 2h. As shown in Fig. 10, the powder XRD patterns demonstrate the retention of framework structure of compound **1** below 260 °C. For compound **2**, the pattern changes when the temperature reaches 280 °C, which indicates that the structure of compound **2** was thermally stable below 260 °C. The powder XRD patterns of compounds **3** and **4** show as the framework remain stable at 220 and 200 °C. It is obvious that the results of X-ray powder diffraction studies for compounds **1–4** are basically corresponding with thermogravimetric analyses.

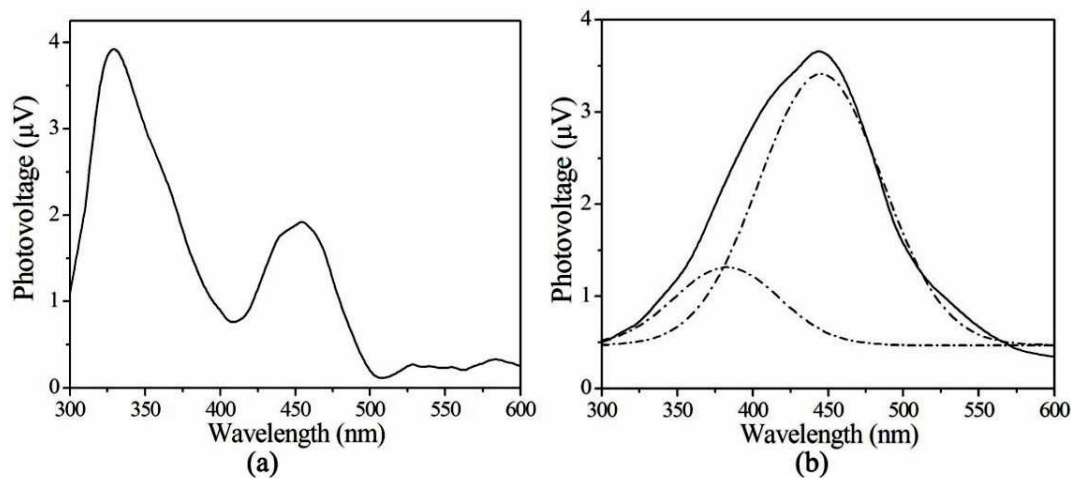


Fig. 11 The SPS of compounds **1** (a) and **3** (b). Dotted lines are treated peak.

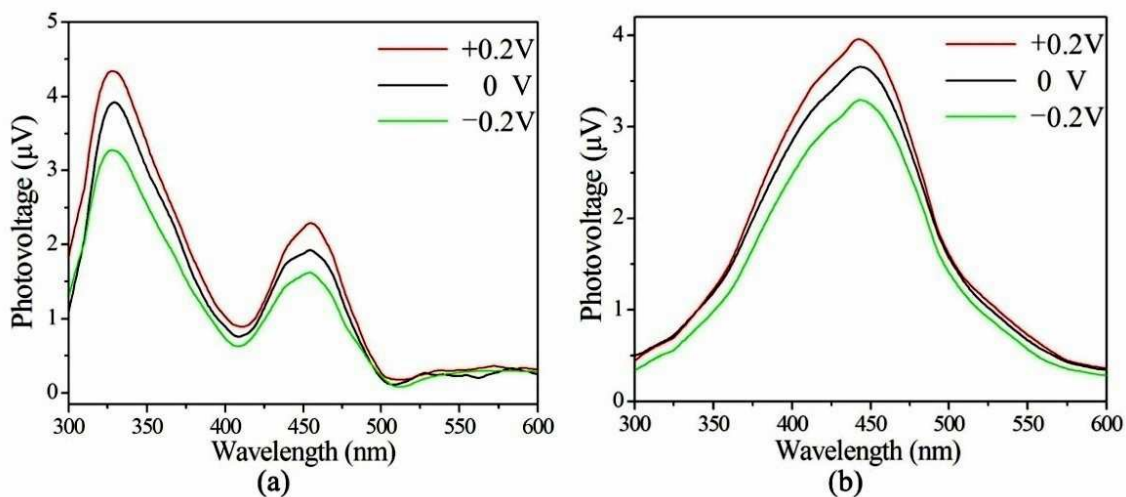


Fig. 12 The FISPS of compounds **1** (a) and **3** (b).

Surface photovoltage properties

In order to continue with exploring functional properties of the compounds, surface photovoltage spectra (SPS) are a well-established contactless and nondestructive technique for the characterization of materials. The principle and the scheme are described elsewhere.^{18,19} The SPS spectra of compounds **1** and **3** were measured in the range of 300–600 nm (Fig. 11). They all appear as positive surface photovoltage (SPV) response bands between 300 and 600 nm. Compound **1** presents two positive SPV responses at 329 and 454 nm (Fig. 11a), and they are assigned to the LMCT (from ligand-to-metal charge transfer) transition. For compound **3**, it can be seen that the SPS signal is a wide peak. The signal is actually the result of overlap of several SPV response bands. To make the assignment of each SPV response band clear, we separated them by the Origin 7.0 program. The compound **3** presents two positive SPV responses at 375 and 445 nm (Fig. 11b). The two response bands are assigned to the LMCT (from ligand-to-metal charge transfer) transition.

On the basis of the principle of SPS, Dr. Wang's group developed a field-induced surface photovoltage technique.^{19, 20} Field-induced surface photovoltage spectroscopy (FISPS) can be measured by applying an external electric field to the sample with a transparent electrode. If a positive electric field is vertically applied on a *p*-type semiconductor surface, the SPV response increases since the external field is consistent with the built-in field. On the contrary, when a negative electric field is applied, the SPV response is weakened. In contrast to *p*-type semiconductors, the SPV response intensity of *n*-type semiconductor increases as a negative field is applied and reduces as a positive electric field is applied. Fig. 12 shows the FISPS of compounds **1** and **3** in the range of 300–600 nm when the external electric fields are -0.2, 0, and +0.2 V, respectively. The SPV response intensities of the two compounds all increase with application of a positive electric field and reduce with application of a negative electric field. This is attributed to the positive electric field being beneficial to the separation of photoexcited electron-hole pairs, which in turn results in an increase of response intensity; however, the negative electric field has just the opposite effect. The FISPS confirm that compounds **1** and **3** show *p*-type semiconductor characteristics.

The surface photovoltage spectra (SPS) and field-induced surface photovoltage spectra (FISPS) of compounds **1** and **3** indicate that they all possess certain photo-electric conversion properties and show *p*-type semiconductor characteristics. These results show that compounds **1** and **3** may be applied as potential inorganic-organic hybrid semiconductor functional materials in the future.

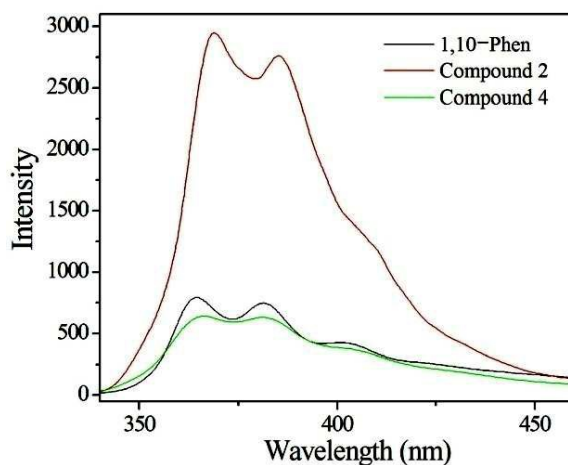


Fig. 13 Solid-state emission spectra of 1, 10-phen (black line), compound **2** (red line) and compound **4** (green line) at room temperature.

Luminescent properties

In recent years, luminescent materials with d^{10} metal centres have attracted much attention due to their potential applications in many fields, such as photochemistry, chemical sensors, and electroluminescent display.²¹ Therefore, solid-state luminescent properties of the free H_2L ligand, 1, 10-phen ligand and compounds **2** and **4** were investigated at room temperature.

The free H_2L ligand exhibits an emission band at 400 nm upon excitation at 290 nm, which displays very weak luminescence in the solid state at room temperature (Fig. S12, ESI). As shown in Fig. 13, the free 1, 10-phen ligand displays luminescence with two emission maxima at 364 nm and 381 nm ($\lambda_{ex} = 280$ nm). The spectra of compounds **2** and **4** are similar to the free 1,10-phen ligand, with a slight red-shift effect, showing the maxima at 368 nm and 384 nm for **2**, and 365 nm and 381 nm for **4** respectively ($\lambda_{ex} = 280$ nm). Because the Zn(II) ions and Cd(II) ions are difficult to oxidize or to reduce, the emissions of these compounds are neither MLCT nor LMCT.^{22, 23} These emission spectra of compounds **2** and **4** can probably be attributed to an intraligand $\pi-\pi^*$ transitions of the phenanthroline ligand, as reported for other zinc(II) and cadmium(II) phosphonates containing N-donor second ligand such as 4,4'-bipy or 1,10-phen.²³⁻²⁵ Moreover, it is clear that a significant enhancement in intensity occur in compound **2**, while compound **4** shows a slightly weakened intensity. The luminescent intensity of compound **2** is stronger than that of compound **4**, which is probably due to the differences of the metal ions. The density of electron cloud for oxygen atoms is closely associated with the coordination of the metal ions.²⁶ Unfortunately, the luminescent

lifetimes of compounds **2** and **4** are not observed, since the lifetimes of compounds **2** and **4** are too short to be measured.

Under similar measurement conditions, the luminescent intensity of compound **2** is more than 3 times larger than that of the free 1, 10-phen ligand which can be attributed to the chelating of 1, 10-phen ligand to the metal centre, which effectively increases its rigidity and asymmetry and reduces the loss of energy by radiationless decay.^{25, 27} The results indicate that the use of the second ligand (1, 10-phen) may be an effective way to prepare luminescent materials.

Conclusions

In this paper, four new transition metal phosphonates with 2D and 3D supramolecular structures, namely, $[\text{Cu}_2(1,10\text{-phen})_2(\text{HL})_2(\text{L})] \cdot \text{H}_2\text{L}$ (**1**), $[\text{Zn}(1,10\text{-phen})(\text{HL})_2]$ (**2**), $[\text{M}(1,10\text{-phen})(\text{HL})_2(\text{H}_2\text{L})]$ ($\text{M} = \text{Mn}$ (**3**), Cd (**4**)), have been synthesized under hydrothermal conditions. In compound **1**, two $\{\text{CuN}_2\text{O}_3\}$ square pyramids and three $\{\text{CPO}_3\}$ tetrahedra are interconnected through phosphonate oxygen atoms to form a cluster unit *via* edge- and corner-sharing. Neighboring units are further assembled into a 3D supramolecular structure through π - π stacking and hydrogen bonding interactions. For compound **2**, two $\{\text{ZnO}_3\text{N}_2\}$ square pyramids and four $\{\text{CPO}_3\}$ tetrahedra are interconnected by phosphonate oxygen atoms to a cluster unit *via* corner-sharing. Then the adjacent clusters are further assembled into a 3D supramolecular structure through π - π stacking interactions. Compounds **3** and **4** are isomorphous and adopt a 2D supramolecular structure. The interconnection of $\{\text{MO}_4\text{N}_2\}$ and $\{\text{CPO}_3\}$ polyhedra leads to a cluster unit through corner-sharing, and such units are further assembled into a 2D supramolecular structure by π - π stacking and hydrogen bonding interactions. The SPS and FISPS of compounds **1** and **3** indicate that they exhibit certain photo-electric conversion properties and show *p*-type semiconductor characteristics. These results show that compounds **1** and **3** may be applied as potential inorganic-organic hybrid semiconductor functional materials in the future. Luminescent properties of compounds **2** and **4** indicate that the use of the second ligand (1, 10-phen) may be an effective way to prepare luminescent materials and compounds **2** and **4** may be candidates for potential luminescent materials.

Acknowledgments

This work is supported by the National Natural Science Foundation of China (Grant No. 21371085).

Notes and references

1. Y. Z. Zhang, P. Ferko, D. Siretanu, R. Ababei, N. P. Rath, M. J. Shaw, R. Clérac, C. Mathonière and S. M. Holmes, *J. Am. Chem. Soc.*, 2014, **136**, 16854; S. S. Hu, J. Y. Li, J. F. Xiang, J. Pan, S. Z. Luo and J. P. Cheng, *J. Am. Chem. Soc.*, 2010, **132**, 7216; D. W. Xu, L. H. Jiang, A. Singh, D. Dustin, M. Yang, L. Liu, R. Lund, T. J. Sellati and H. Dong, *Chem. Commun.*, 2015, **51**, 1289; V. Ramamurthy and S. Gupta, *Chem. Soc. Rev.*, 2015, **44**, 119; (e) J. Voskuhl, S. Sankaran and P. Jonkheijm, *Chem. Commun.*, 2014, **50**, 15144.
2. N. Vallavoju and J. Sivaguru, *Chem. Soc. Rev.*, 2014, **43**, 4084; Y. S. Ma, X. Y. Tang, W. Y. Yin, B. Wu, F. F. Xue, R. X. Yuan and S. Roy, *Dalton Trans.*, 2012, **41**, 2340; X. P. Yang, B. P. Hahn, R. A. Jones, W. K. Wong and K. J. Stevenson, *Inorg. Chem.*, 2007, **46**, 7050; P. Yang, J. J. Wu, H. Y. Zhou and B. H. Ye, *Cryst. Growth Des.*, 2012, **12**, 99.
3. A. Clearfield and K. Demadis, *Metal Phosphonate Chemistry: From Synthesis to Applications*, Published by the Royal Society of Chemistry, Oxford, 2012, p. 164; F. P. Zhai, Q. S. Zheng, Z. X. Chen, Y. Ling, X. F. Liu, L. H. Weng and Y. M. Zhou, *CrystEngComm.*, 2013, **15**, 2040; L. H. Schilling and N. Stock, *Dalton Trans.*, 2014, **43**, 414; S. F. Tang, L. J. Li, X. X. Lv, C. Wang and X. B. Zhao, *CrystEngComm.*, 2014, **16**, 7043.
4. Z. Y. Du, H. B. Xu, X. L. Li and J. G. Mao, *Eur. J. Inorg. Chem.*, 2007, 4520; K. D. Demadis, A. Panera, Z. Anagnostou, D. Varouhas, A. M. Kirillov and I. Císařová, *Cryst. Growth Des.*, 2013, **13**, 4480; M. Taddei, F. Costantino, R. Vivani, C. Sangregorio, L. Sorace and L. Castelli, *Cryst. Growth Des.*, 2012, **12**, 2327; T. T. Wang, M. Ren, S. S. Bao, B. Liu, L. Pi, Z. S. Cai, Z. H. Zheng, Z. L. Xu and L. M. Zheng, *Inorg. Chem.*, 2014, **53**, 3117.
5. A. Bulut, Y. Zorlu, R. Topkaya, B. Aktaş, S. Doğan, H. Kurt and G. Yücesan, *Dalton Trans.*, 2015, **44**, 12526; F. Tong, Z. G. Sun, K. Chen, Y. Y. Zhu, W. N. Wang, C. Q. Jiao, C. L. Wang and C. Li, *Dalton Trans.*, 2011, **40**, 5059; M. J. Zheng, Y. Y. Zhu, Z. G. Sun, J. Zhu, C. Q. Jiao, W. Chu, S. H. Sun and H. Tian, *CrystEngComm.*, 2013, **15**, 1445.

6. R. Clarke, K. Latham, C. Rix, M. Hobday and J. White, *CrystEngComm*, 2004, **6**, 42; K. Latham, A. M. Coyle, C. J. Rix, A. Fowless and J. M. White, *Polyhedron*, 2007, **26**, 222; K. Latham, K. F. White, K. B. Szpakolski, C. J. Rix and J. M. White, *Inorganica Chimica Acta*, 2009, **362**, 1872.
7. V. Chandrasekhar, J. Goura and E. C. Sañudo, *Inorg. Chem.*, 2012, **51**, 8479; J. A. Sheikh, A. Adhikary, H. S. Jena, S. Biswas and S. Konar, *Inorg. Chem.*, 2014, **53**, 1606; B. K. Tripuramallu, S. Mukherjee and S. K. Das, *Cryst. Growth Des.*, 2012, **12**, 5579.
8. L. Kronik and Y. Shapira, *Surf. Sci. Rep.*, 1999, **37**, 1; Y. Zidon, Y. Shapira, H. Shaim and T. Dittrich, *Appl. Surf. Sci.*, 2008, **254**, 3255.
9. C. Li, C. Q. Jiao, Z. G. Sun, K. Chen, C. L. Wang, Y. Y. Zhu, J. Zhu, Y. Zhao, M. J. Zheng, S. H. Sun, W. Chu and H. Tian, *CrystEngComm.*, 2012, **14**, 5479; S. H. Sun, Z. G. Sun, Y. Y. Zhu, D. P. Dong, C. Q. Jiao, J. Zhu, J. Li, W. Chu, H. Tian, M. J. Zheng, W. Y. Shao and Y. F. Lu, *Cryst. Growth Des.*, 2013, **13**, 226 ; D. P. Dong, Z. G. Sun, F. Tong, Y. Y. Zhu, K. Chen, C. Q. Jiao, C. L. Wang, C. Li and W. N. Wang, *CrystEngComm.*, 2011, **13**, 3317.
10. G. M. Sheldrick, *Acta Crystallogr. Sect. A: Found. Crystallogr.*, 2008, **64**, 112.
11. S. Ushak, E. Spodine, E. L. Fur, D. Venegas–Yazigi, J.–Y. Pivan, W. Schnelle, R. Cardoso–Gil and R. Kniep, *Inorg. Chem.*, 2006, **45**, 5393.
12. C. Janiak, *J. Chem. Soc., Dalton Trans.*, 2000, 3885; W. Zhou, Y. Y. Zhu, C. Q. Jiao, Z. G. Sun, S. P. Shi, L. L. Dai, T. Sun, W. Z. Li, M. X. Ma and H. Luo, *CrystEngComm.*, 2014, **16**, 1174.
13. R. B. Fu, S. M. Hu and X. T. Wu, *CrystEngComm.*, 2013, **15**, 8937.
14. Z. Y. Du, A. V. Prosvirin and J. G. Mao, *Inorg. Chem.*, 2007, **46**, 9884.
15. L. L. Dai, Y. Y. Zhu, C. Q. Jiao, Z. G. Sun, S. P. Shi, W. Zhou, W. Z. Li, T. Sun, H. Luo and M. X. Ma, *CrystEngComm.*, 2014, **14**, 5050.
16. R. C. Clarke, K. Latham, C. J. Rix and M. Hobday, *Chem. Mater.*, 2004, **16**, 2463; K. P. Rao and K. Vidyasagar, *Eur. J. Inorg. Chem.*, 2005, 4936.
17. A. Cabeza, X. Ouyang, C. V. K. Sharma, M. A. G. Aranda, S. Bruque and A. Clearfield, *Inorg. Chem.*, 2002, **41**, 2325.
18. J. Zhang, D. J. Wang, Y. M. Chen, T. J. Li, H. F. Mao, H. J. Tian, Q. F. Zhou and H. J. Xu, *Thin Solid Films.*, 1997, **300**, 208; L. Q. Jing, X. J. Sun, J. Shang, W. M. Cai, Z. L. Xu, Y. G. Du and H. G. Fu, *Sol Energ Mat Sol C.*, 2003, **97**, 133.

19. Y. H. Lin, D. J. Wang, Q. D. Zhao, M. Yang and Q. L. Zhang, *J. Phys. Chem. B.*, 2004, **108**, 3202.
20. D. J. Wang, J. Zhang, T. S. Shi, B. H. Wang, X. Z. Cao and T. J. Li, *J. Photochem. Photobiol. A: Chem.*, 1996, **93**, 21.
21. J. E. McGarrah, Y. J. Kim, M. Hissler and R. Eisenberg, *Inorg. Chem.*, 2001, **40**, 4510; B. An, R. Zhou, D. Dang, J. Wang, H. Pan and Y. Bai, *Spectrochim. Acta A*, 2014, **122**, 392; M. Zhang, Y. Ren and X. Chen, *J. Mol. Struct.*, 2014, **1075**, 7.
22. L. F. Ma, C. P. Li, L. Y. Wang and M. Du, *Cryst. Growth Des.*, 2010, **10**, 2641.
23. W. Q. Kan, J. F. Ma, Y. Y. Liu, J. Yang and B. Liu, *CrystEngComm*, 2012, **14**, 2268.
24. J. L. Song, H. H. Zhao, J. G. Mao and K. R. Dunbar, *Chem. Mater.*, 2004, **16**, 1884.
25. E. Fernández-Zapico, J. Montejo-Bernardo, A. Fernández-González, J. R. García and S. García-Granda, *J. Solid State Chem.*, 2015, **225**, 285.
26. H. Y. Wang, S. Gao, L. H. Huo, S. W. Ng and J. G. Zhao, *Cryst. Growth Des.*, 2008, **8**, 665.
27. S. Wang, *Coord. Chem. Rev.*, 2001, **215**, 79.

